
PERGAMON

Journal of the Mechanics and Physics of Solids
50 (2002) 583–613

JOURNAL OF THE
MECHANICS AND
PHYSICS OF SOLIDS

www.elsevier.com/locate/jmps

Steady-state mode I cracks in a viscoelastic triangular lattice

Leonid Pechenik[a,1], Herbert Levine[a], David A. Kessler[b,*]

[a] *Department of Physics, University of California, San Diego, La Jolla, CA 92093-0319, USA*
[b] *Department of Physics, Bar-Ilan University, Ramat-Gan, Israel*

Received 15 September 2000; received in revised form 7 April 2001; accepted 7 April 2001

Abstract

We construct exact solutions for Mode I steady-state cracks in an ideally brittle viscoelastic triangular lattice model. Our analytic solutions for the infinite lattice are compared to numerical results for finite width systems. The issues we address include the crack velocity versus driving curve as well as the onset of additional bond breaking, signaling the emergence of complex spatio-temporal behavior. Somewhat surprisingly, the critical velocity for this transition becomes a decreasing function of the dissipation for sufficiently large values thereof. Lastly, we briefly discuss the possible relevance of our findings for experiments on mode I crack instabilities.

Keywords: A. Crack propagation and arrest; A. Dynamic fracture; A. Crack branching and bifurcation

1. Introduction

Recent experiments on dynamical fracture (Fineberg et al., 1991, 1992) have highlighted the fact that cracks in brittle materials become unstable above a critical velocity. This instability is associated with the formation of a roughened fracture surface, with an increased dissipation of elastic energy, and with complicated velocity dynamics—for a review, see (Fineberg and Marder, 1999). Although there are hints of such an instability in the traditional continuum formulations of ideally brittle cracks (Yoffe, 1951), a systematic treatment does not appear possible. Indeed, recent attempts (Langer and Lobkovsky, 1998) to utilize a cohesive stress modification (Barenblatt, 1959) of

* Corresponding author. Fax: +972-3-535-3298.
E-mail addresses: kessler@dave.ph.biu.ac.il (D.A. Kessler), hlevine@ucsd.edu (H. Levine).
[1] Current address: Department of Physics, University of California, Santa Barbara, CA 93106-9530, USA.

0022-5096/02/$ - see front matter
PII: S0022-5096(01)00061-8

the continuum elastic equations in order to address this problem have been rather unsuccessful.

In the absence of a compelling continuum approach, one must deal in some manner with discrete dynamics on the "atomic scale". In this regard, Slepyan (Kulamekhtova et al., 1984; Slepyan, 1981, 1982) pioneered the idea of studying lattice models in which atoms interact (via piece-wise linear springs) with their neighbors in a predetermined lattice geometry. This conceptual framework was further developed by Marder and collaborators (Marder and Gross, 1995; Marder and Liu, 1993). Here, one can directly obtain the relationship between the crack tip velocity and the imposed driving and furthermore one can search for conditions that do not allow stable steady crack motion. Clearly, lattice models are not fully realistic, especially at displacements that are not small compared to the underlying lattice spacing; to be more realistic, one must resort to molecular dynamics simulations including all possible atomic interactions (Abraham et al., 1994; Gumbsch et al., 1997; Holland and Marder, 1997, 1998; Omeltchenko et al., 1997; Zhou et al., 1997). However, the analytic tractability of these models as well as indications (Marder and Gross, 1995; Pla et al., 1998; Sander and Ghasias, 1999) that they do contain the essential mechanism responsible for the observed dynamical instability make them well worthy of serious attention.

Slepyan recognized that in an ideally brittle material (where each spring is linear until a displacement at which it completely breaks) one can use Fourier methods to find the lattice analog of a traveling wave solution. In this solution, each point on the lattice (at the same transverse coordinate) undergoes the same time history of motion as any other, albeit with some time delay. Once one obtains the solution, one must check that all springs assumed to be linear have displacements that are in fact below the breaking threshold. The violation of this assumption by the steadily propagating solution signals the onset of more complex dynamical behavior, at least in qualitative accord to what is seen experimentally (Fineberg and Marder, 1999; Marder and Gross, 1995). Using the Wiener–Hopf technique, Slepyan solved for the velocity–driving curve in the limit where the width of the lattice transverse to the crack direction goes to infinity.

One important consideration in all models of brittle fracture concerns dissipation mechanisms. Dissipation introduces a new velocity scale into the problem and it is therefore interesting to investigate how this can influence crack dynamics. Apart from this, local dissipation might be used in a phenomenological approach to mimic other effects (such as the creation of bound dislocations) absent from the basic lattice treatment. From our perspective, it makes sense to put in dissipation at the lattice scale in such a way so as not to dominate the large-scale continuum elastic field. If in addition one demands an equation that is local in time, one is led (Langer, 1992; Pla et al., 1998) to the introduction of a Kelvin viscosity which dissipates energy proportional to the rate of change of spring lengths. In the naive continuum limit, this gives rise to a third derivative (two space, one time) term. That means that if the viscosity is chosen to be O(1) on the lattice scale, it will scale to zero as far as the macroscopic dynamics is concerned. We saw this explicitly in a previous set of papers (Kessler, 2000; Kessler and Levine, 1998), which solved this problem for finite width lattices and considered the nature of the solution as the width became large. Nevertheless, the

viscosity can have a considerable effect on aspects of the solution that depend on the microscopic details, namely the crack speed (for a fixed stress intensity factor) and the self-consistency of the traveling wave ansatz.

In this paper, we extend the methodology originally devised by Slepyan (1981) and obtain a closed form solution for Mode I cracks propagating steadily in a triangular lattice in the presence of dissipation in the form of a Kelvin viscosity. This type of term maintains the exact solvability of the model while, as already mentioned above, restricting the dissipation to occur only inside the process zone. This latter requirement is not met by the more typical Stokes viscosity term (Marder and Gross, 1995) which is more effective in damping motion on large scales than it is on the scale of the crack tip. Via our exact solution, we determine the effect of dissipation on the crack velocity as a function of driving. We find the critical velocity (and the associated critical time) at which other bonds in the lattice have displacements larger than the assumed breaking criterion, signaling an instability in the steadily propagating crack and the onset of more complex spatio-temporal behavior. We also solve the same system numerically on a lattice of finite transverse extent so as to provide an independent check on some of the results.

Perhaps the most interesting finding reported here concerns the aforementioned onset of additional bond-breaking at large enough velocity. At small dissipation, diagonal bonds that are offset from the assumed crack line in the vertical direction are the most "dangerous". The critical velocity at which one of these bonds exceeds critical displacement is more or less independent of the dissipation at low values thereof and eventually rises sharply as the system becomes increasingly damped. At moderate to large damping, however, horizontal bonds become more relevant and eventually give rise to a critical velocity that decreases with increasing damping. This is unlike what happens in mode III cracks on a square lattice, a system studied by us (Pechenik, 2000) and also by Slepyan and co-workers (Slepyan et al., 1999). At the end, we will comment on the possible relevance of our results for trying to make sense of recent experiments (Fineberg et al., 1991, 1992; Sharon et al., 1995, 1996) and simulations on instabilities during dynamic fracture.

2. Mode I on a triangular lattice

Our model consists of central force springs between mass points located on a triangular lattice. We introduce unit vectors in the lattice directions as follows: $\hat{d}_1$ points in the direction of the x-axis and each of the subsequent unit vectors $\hat{d}_i$ with $2 \leqslant i \leqslant 6$ rotated by an additional $\pi/3$ in the counter-clockwise direction. This means that $\hat{d}_{i+3} = -\hat{d}_i$. We will always assume that the steady-state crack breaks bonds between the rows with $y = 0$ and $\sqrt{3}/2$, as it moves in the direction of the x-axis. This geometry is indicated in Fig. 1, where the next bond to break is labeled "b". Following Slepyan, we take each bond in our lattice to be linear until a critical displacement, 2ε, at which point it completely breaks. Also, dissipation is incorporated as a Kelvin viscosity term, with each (uncracked) spring having a viscous damping η. Given these assumptions, the

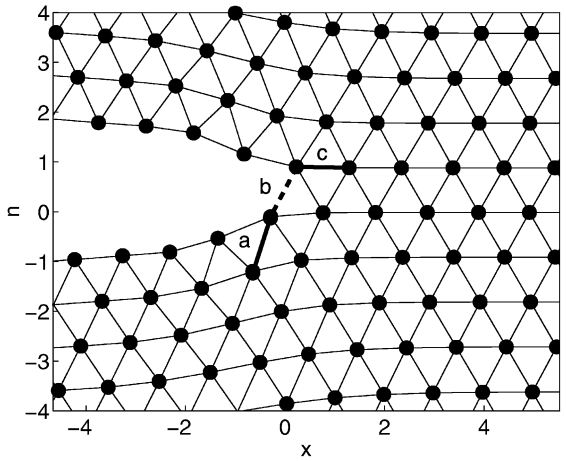

Fig. 1. Lattice geometry of the region around the tip of the crack.

equation describing the motion of the masses in the lattice is

$$\left(1+\eta\frac{\partial}{\partial t}\right)\sum_{i=1}^{6}Q_i(t,\vec{x})\hat{d}_i-\frac{\partial^2\vec{u}}{\partial t^2}=-\vec{\sigma}(t,\vec{x}). \tag{1}$$

Here, $\vec{x}=(x,y)$ is a lattice vector in the plane and $Q_i(t,\vec{x})$ is the elongation of bond i emanating from the specific lattice site, in the approximation that this elongation is much smaller than the unstretched bond length,

$$Q_i(t,\vec{x})=(\vec{u}(t,\vec{x}+d_i)-\vec{u}(t,\vec{x}))\cdot\hat{d}_i. \tag{2}$$

Finally, the driving term $\vec{\sigma}(t,\vec{x})$ consists of forces that compensate for the forces from broken bonds (which are included on the left-hand side) as well as any external forces acting on the crack boundaries.

Next, we suppose that the crack is moving with a constant speed v. This allows us to change variables to $\tau=x-vt$, $\vec{z}=(\tau,y)$, which gives

$$\left(1+\eta v\frac{\partial}{\partial\tau}\right)\sum_{i=1}^{6}Q_i(\vec{z})\hat{d}_i-v^2\frac{\partial^2\vec{u}}{\partial\tau^2}=-\vec{\sigma}(\vec{z}). \tag{3}$$

Because of the form of $Q_i(\vec{z})$, we have the obvious symmetries

$$Q_2(\vec{z})=Q_5(\vec{z}+\hat{d}_2),\quad Q_3(\vec{z})=Q_6(\vec{z}+\hat{d}_3). \tag{4}$$

We will impose one additional symmetry condition on the Q_i. As the crack propagates, it alternately breaks bonds in the $\hat{d}_2$ and $\hat{d}_3$ directions. Let us define our coordinates such that at $\tau=0$ and $t=0$, (so that $x=0$), the crack breaks a bond in the direction of $\hat{d}_2$. This means that for $\tau>0$ this bond ($Q_2(\vec{z}_0)$ with $\vec{z}_0=(\tau,0)$) is unbroken and for $\tau<0$ it is always broken. If we shift one lattice spacing to the left, the $\hat{d}_2$ bond at $x=-1$ will break at $t=-1/v$ (here also $\tau=0$ in $Q_2(\vec{z}_0)$). It is clear that

the bond in the $\hat{d}_3$ direction at $x=0$ breaks at a time-point between these two events; we will assume that this time is exactly at the midpoint, $t=-1/(2v)$ or equivalently $\tau=1/2$ in $Q_3(\vec{z}_0)$. This means that for $\tau>1/2$ this bond is unbroken and for $\tau<1/2$ it is always broken. We will assume an even more strict symmetry condition for these bonds, namely

$$Q_2(\vec{z}_0)=Q_3\left(x-v\left(t-\frac{1}{2v}\right),y=0\right)=Q_5\left(\vec{z}_0+\frac{1}{2}\hat{d}_1\right), \tag{5}$$

which will need to be checked from our solution later.

Let us denote $Q_2(\vec{z}_0)\equiv Q(\tau)$. Then, we can write down an explicit expression for the forces $\vec{\sigma}(\vec{z})$ on the right-hand side of Eq. (3). For the row with $y=0$

$$\begin{aligned}\vec{\sigma}(\vec{z}_0)&=\theta(-\tau)\left(\vec{\sigma}_e(\vec{z}_0)-\left(1-\eta v\frac{\partial}{\partial\tau}\right)Q_2(\vec{z}_0)\hat{d}_2\right)\\&\quad+\theta\left(-\tau+\frac{1}{2}\right)\left(\vec{\sigma}'_e(\vec{z}_0)-\left(1-\eta v\frac{\partial}{\partial\tau}\right)Q_3(\vec{z}_0)\hat{d}_3\right) \qquad (6)\\&=\theta(-\tau)\left(-P_0(\tau)-\left(1-\eta v\frac{\partial}{\partial\tau}\right)Q(\tau)\right)\hat{d}_2\\&\quad+\theta\left(-\tau+\frac{1}{2}\right)\left(-P_0\left(\tau-\frac{1}{2}\right)-\left(1-\eta v\frac{\partial}{\partial\tau}\right)Q\left(\tau-\frac{1}{2}\right)\right)\hat{d}_3. \qquad (7)\end{aligned}$$

Here $\vec{\sigma}_e$ and $\vec{\sigma}'_e$ are the assumed external forces. In the second form, these have been taken to match the vectorial nature and also the symmetry of the bond-breaking terms. The (scalar) P_0 will be specified later. Note that the second theta function in Eq. (6) reflects the already mentioned fact that the bond from the point $\vec{z}_0$ in the $\hat{d}_3$ direction breaks earlier (by the amount $1/2v$) than the bond from the same point in the $\hat{d}_2$ direction.

Let us write down the corresponding force for the row $y=\sqrt{3}/2$. For the point $\vec{x}=\hat{d}_2$, the bond in the $\hat{d}_5$ direction is physically the same as the $\hat{d}_2$ bond at $\vec{x}=(0,0)$ and therefore breaks at $\tau=0$ in $Q_5(\vec{z}_0+\hat{d}_2)=Q_2(\vec{z}_0)$. Now, the $\hat{d}_6$ bond at $\vec{x}=\hat{d}_2$ breaks later, at $\tau=-1/2$ in $Q_6(\vec{z}_0+\hat{d}_2)$. Thus we have

$$\begin{aligned}\vec{\sigma}(\vec{z}_0+d_2)&=\theta(-\tau)\left(\vec{\sigma}_e(\vec{z}_0+d_2)-\left(1-\eta v\frac{\partial}{\partial\tau}\right)Q_2(\vec{z}_0+d_2)\hat{d}_5\right)\\&\quad+\theta\left(-\tau-\frac{1}{2}\right)\left(\vec{\sigma}'_e(\vec{z}_0+d_2)-\left(1-\eta v\frac{\partial}{\partial\tau}\right)Q_3(\vec{z}_0+d_2)\hat{d}_6\right) \qquad (8)\\&=\theta(-\tau)\left(-P_0(\tau)-\left(1-\eta v\frac{\partial}{\partial\tau}\right)Q(\tau)\right)\hat{d}_5\\&\quad+\theta\left(-\tau-\frac{1}{2}\right)\left(-P_0\left(\tau+\frac{1}{2}\right)-\left(1-\eta v\frac{\partial}{\partial\tau}\right)Q\left(\tau+\frac{1}{2}\right)\right)\hat{d}_6. \qquad (9)\end{aligned}$$

where we used the symmetry in Eq. (5) to write $Q_6(\vec{z}_0+\hat{d}_2)=Q_3(\vec{z}_0+\hat{d}_2-\hat{d}_3)=Q_2(\vec{z}_0+\hat{d}_2-\hat{d}_3-\hat{d}_1/2)=Q(\tau+1/2)$. Finally, we can rewrite all these forces in a more compact

form,

$$\vec{\sigma}(\vec{z}_0) = N(\tau)\hat{d}_5 + N\left(\tau - \tfrac{1}{2}\right)\hat{d}_6, \tag{10}$$

$$\vec{\sigma}(\vec{z}_0 + \hat{d}_2) = N(\tau)\hat{d}_2 + N\left(\tau + \tfrac{1}{2}\right)\hat{d}_3, \tag{11}$$

where

$$N(\tau) = \theta(-\tau)\left(-P_0(\tau) - \left(1 - \eta v\frac{\partial}{\partial\tau}\right)Q(\tau)\right). \tag{12}$$

Next, we proceed by performing a Fourier transformation of Eq. (3), over the continuous variable τ and the discrete variable $y = n\sqrt{3}/2$, with integer n. In detail

$$u^{\mathrm{F}}(\tau, s) = \sum_{n=-\infty}^{\infty} u\left(\tau, \frac{\sqrt{3}}{2}n\right)\mathrm{e}^{\mathrm{i}(\sqrt{3}/2)sn}, \tag{13a}$$

$$u(\tau, y) = \frac{\sqrt{3}}{4\pi}\int_{-2\pi/\sqrt{3}}^{2\pi\sqrt{3}} \mathrm{d}s u^{\mathrm{F}}(\tau, s)\mathrm{e}^{-\mathrm{i}sy}, \tag{13b}$$

$$u^{\mathrm{FF}}(q, s) = \int_{-\infty}^{\infty} \mathrm{d}\tau u^{\mathrm{F}}(\tau, s)\mathrm{e}^{\mathrm{i}q\tau}, \tag{14a}$$

$$u^{\mathrm{F}}(\tau, s) = \frac{1}{2\pi}\int_{-\infty}^{\infty} \mathrm{d}q u^{\mathrm{FF}}(q, s)\mathrm{e}^{-\mathrm{i}q\tau}. \tag{14b}$$

We thereby obtain

$$-v^2q^2u^{\mathrm{FF}} - (1 + \mathrm{i}\eta vq)\sum_i Q_i^{\mathrm{FF}}\hat{d}_i = \vec{\sigma}^{\mathrm{FF}} \tag{15}$$

with

$$Q_i^{\mathrm{FF}} = (\mathrm{e}^{-\mathrm{i}\vec{r}\cdot\vec{d}_i} - 1)\vec{u}^{\,\mathrm{FF}} \cdot \hat{d}_i \tag{16}$$

and $\vec{r} = (q, s)$.

To find $\vec{\sigma}^{\mathrm{FF}}$ we first transform Eqs. (10), (11) over τ:

$$\vec{\sigma}^{\mathrm{F}}(q, n = 0) = N(q)\hat{d}_5 + \mathrm{e}^{\mathrm{i}q/2}N(q)\hat{d}_6, \tag{17a}$$

$$\vec{\sigma}^{\mathrm{F}}(q, n = 1)\mathrm{e}^{-\mathrm{i}q/2} = N(q)\hat{d}_2 + \mathrm{e}^{-\mathrm{i}q/2}N(q)\hat{d}_3 \tag{17b}$$

with

$$N(q) = P_0^- + (1 + \mathrm{i}\eta vq)Q^- - \eta vQ(0). \tag{18}$$

The superscript "–" refers to the part of the Fourier transform which is analytic in the lower half plane of the variable q; see the appendix for details on our notations

and conventions. Finally, using Eq. (13a) we get

$$\vec{\sigma}^{\mathrm{FF}} = N(q)\hat{d}_5 + \mathrm{e}^{\mathrm{i}q/2}N(q)\hat{d}_6 + (\mathrm{e}^{\mathrm{i}q/2}N(q)\hat{d}_2 + N(q)\hat{d}_3)\mathrm{e}^{\mathrm{i}s\sqrt{3}/2}. \tag{19}$$

This then completes the derivation of the basic equation that needs to be solved to determine the steady-state crack field.

3. Wiener–Hopf solution

We wish to use the Wiener–Hopf technique to solve the equation derived above for the elongation field Q. To start, we note that Eq. (15) can be written in matrix form

$$\boldsymbol{M}\vec{u}^{\,\mathrm{FF}} = \vec{\sigma}^{\mathrm{FF}} \tag{20}$$

with the 2×2 matrix

$$\boldsymbol{M} = \begin{pmatrix} A_1 & A_3 \\ A_3 & A_2 \end{pmatrix} \tag{21}$$

where

$$A_1 = -v^2q^2 + (1 + \mathrm{i}\eta vq)\left(4\sin^2\frac{\vec{r}\cdot\hat{d}_1}{2} + \sin^2\frac{\vec{r}\cdot\hat{d}_2}{2} + \sin^2\frac{\vec{r}\cdot\hat{d}_3}{2}\right), \tag{22a}$$

$$A_2 = -v^2q^2 + 3(1 + \mathrm{i}\eta vq)\left(\sin^2\frac{\vec{r}\cdot\hat{d}_2}{2} + \sin^2\frac{\vec{r}\cdot\hat{d}_3}{2}\right), \tag{22b}$$

$$A_3 = \sqrt{3}(1 + \mathrm{i}\eta vq)\left(\sin^2\frac{\vec{r}\cdot\hat{d}_2}{2} - \sin^2\frac{\vec{r}\cdot\hat{d}_3}{2}\right), \tag{22c}$$

and

$$\vec{\sigma}^{\mathrm{FF}} = -\frac{N(q)}{2}\begin{pmatrix} (1 - \mathrm{e}^{\mathrm{i}q/2})(1 + \mathrm{e}^{\mathrm{i}(\sqrt{3}/2)s}) \\ \sqrt{3}(1 + \mathrm{e}^{\mathrm{i}q/2})(1 - \mathrm{e}^{\mathrm{i}(\sqrt{3}/2)s}) \end{pmatrix}. \tag{23}$$

The solution of Eq. (20) is therefore

$$\vec{u}^{\,\mathrm{FF}} = \frac{1}{\det \boldsymbol{M}}\begin{pmatrix} \det \boldsymbol{M}_1 \\ \det \boldsymbol{M}_2 \end{pmatrix} \tag{24}$$

where

$$\boldsymbol{M}_1 = \begin{pmatrix} \sigma_x^{\mathrm{FF}} & \sigma_y^{\mathrm{FF}} \\ A_3 & A_2 \end{pmatrix}, \qquad \boldsymbol{M}_2 = \begin{pmatrix} A_1 & A_3 \\ \sigma_x^{\mathrm{FF}} & \sigma_x^{\mathrm{FF}} \end{pmatrix}. \tag{25}$$

Now, we want to extract from the solution Eq. (24) an equation for the variable we are interested in, namely $Q^{\mathrm{F}}(q)$. From the definition of Q we have

$$Q^{\mathrm{F}}(q) = Q_2^{\mathrm{F}}(q, n=0) = \frac{\sqrt{3}}{4\pi} \int_{-2\pi/\sqrt{3}}^{2\pi/\sqrt{3}} \mathrm{d}s(\mathrm{e}^{-\mathrm{i}\vec{r}\cdot\vec{d}_2} - 1)\vec{u}^{\,\mathrm{FF}} \cdot \hat{d}_2. \tag{26}$$

From the basic solution above, we can evaluate $\vec{u}^{\,\mathrm{FF}} \cdot \hat{d}_2$:

$$\vec{u}^{\,\mathrm{FF}} \cdot \hat{d}_2 = \frac{\begin{vmatrix} -d_{2x}A_3 + d_{2y}A_1 & -d_{2x}A_2 + d_{2y}A_3 \\ \sigma_x^{\mathrm{FF}} & \sigma_y^{\mathrm{FF}} \end{vmatrix}}{|\boldsymbol{M}|}. \tag{27}$$

Before proceeding to evaluate the integral, it is worthwhile to pause and check the basic symmetry conditions. We find that

$$Q_3^{\mathrm{F}}(q, n=0) = \frac{\sqrt{3}}{4\pi} \int_{-2\pi/\sqrt{3}}^{2\pi/\sqrt{3}} \mathrm{d}s(\mathrm{e}^{-\mathrm{i}\vec{r}\cdot\vec{d}_3} - 1)\vec{u}^{\,\mathrm{FF}} \cdot \hat{d}_3, \tag{28}$$

where the new dot product $\vec{u}^{\,\mathrm{FF}} \cdot \hat{d}_3$ is given by

$$\vec{u}^{\,\mathrm{FF}} \cdot \hat{d}_3 = \frac{\begin{vmatrix} d_{2x}A_3 + d_{2y}A_1 & d_{2x}A_2 + d_{2y}A_3 \\ \sigma_x^{\mathrm{FF}} & \sigma_y^{\mathrm{FF}} \end{vmatrix}}{|\boldsymbol{M}|}. \tag{29}$$

Now, we can change variables of integration in Eq. (28) from s to $-s$. Under this transformation, $A_1|_{s\to -s} = A_1$, $A_2|_{s\to -s} = A_2$, $A_3|_{s\to -s} = -A_3$, $\sigma_x^{\mathrm{FF}}|_{s\to -s} = \mathrm{e}^{-\mathrm{i}\sqrt{3}s/2}\sigma_x^{\mathrm{FF}}$, $\sigma_y^{\mathrm{FF}}|_{s\to -s} = -\mathrm{e}^{-\mathrm{i}\sqrt{3}s/2}\sigma_y^{\mathrm{FF}}$, which gives that $\det \boldsymbol{M}|_{s\to -s} = \det \boldsymbol{M}$ and $\vec{u}^{\,\mathrm{FF}} \cdot \hat{d}_3|_{s\to -s} = -\mathrm{e}^{-\mathrm{i}\sqrt{3}s/2}\vec{u}^{\,\mathrm{FF}} \cdot \hat{d}_2$. Therefore Eq. (28) changes into

$$\begin{aligned} Q_3^{\mathrm{F}}(q, n=0) &= -\frac{\sqrt{3}}{4\pi} \int_{-2\pi/\sqrt{3}}^{2\pi/\sqrt{3}} \mathrm{d}s(\mathrm{e}^{\mathrm{i}qd_{2x} + \mathrm{i}sd_{2y}} - 1)\mathrm{e}^{-\mathrm{i}d_{2y}s}\vec{u}^{\,\mathrm{FF}} \cdot \hat{d}_2 \\ &= \mathrm{e}^{\mathrm{i}q/2} Q_2^{\mathrm{F}} \quad (q, n=0). \end{aligned} \tag{30}$$

This is exactly the symmetry condition Eq. (5); hence, our solution is consistent with the assumed symmetry. We also note here that a similar derivation gives

$$Q_2(\tau, y) = Q_3\left(\tau + \frac{1}{2}, -y\right) = Q_6\left(\tau + \frac{1}{2}, -y + \frac{\sqrt{3}}{2}\right). \tag{31}$$

More generally, we can see what these symmetries mean for the displacement field $\vec{u}(z)$. Using $\det \boldsymbol{M}_1|_{s\to -s} = \mathrm{e}^{-\mathrm{i}\sqrt{3}s/2} \det \boldsymbol{M}_1$, $\det \boldsymbol{M}_2|_{s\to -s} = -\mathrm{e}^{-\mathrm{i}\sqrt{3}s/2} \det \boldsymbol{M}_2$, we obtain $u_x^{\mathrm{FF}}|_{s\to -s} = \mathrm{e}^{-\mathrm{i}\sqrt{3}s/2}u_x^{\mathrm{FF}}$ and $u_y^{\mathrm{FF}}|_{s\to -s} = -\mathrm{e}^{-\mathrm{i}\sqrt{3}s/2}u_y^{\mathrm{FF}}$. These give $u_x(\tau, y) = u_x(\tau, -y + \sqrt{3}/2)$ and $u_y(\tau, y) = -u_y(\tau, -y + \sqrt{3}/2)$.

We now proceed to calculate the integral in Eq. (26). The explicit form of the integrand in Eq. (26) is

$$\frac{N(q)}{|\det \boldsymbol{M}|}\begin{vmatrix} 3\left(v^2q^2-(1+\mathrm{i}\eta vq)\left(2\sin^2\frac{q}{2}+\sin^2\frac{\vec{r}\cdot\hat{d}_3}{2}\right)\right) \\ -\frac{v^2q^2}{2}+3(1+\mathrm{i}\eta vq)\sin^2\frac{\vec{r}\cdot\hat{d}_3}{2} \\ (\cos\vec{r}\cdot\hat{d}_2-1)-\left(\cos\frac{\sqrt{3}}{2}s-\cos\frac{q}{2}\right) \\ (\cos\vec{r}\cdot\hat{d}_2-1)+\left(\cos\frac{\sqrt{3}}{2}s-\cos\frac{q}{2}\right) \end{vmatrix}. \tag{32}$$

As $|\boldsymbol{M}|$ is an even function of s, only the even part of the other determinant contributes to the integral. Then, by the change of variable to $w=\mathrm{e}^{-\mathrm{i}\sqrt{3}s/2}$ we can rewrite Eq. (26) as an integral over the unit circle in the complex w plane. After some tedious algebra, we find that we can write

$$\det \boldsymbol{M}=3\xi^2+\alpha\xi+\beta, \tag{33}$$

where

$$\xi=\frac{1}{2}(1+\mathrm{i}\eta vq)\left(\frac{1}{w}+w\right), \tag{34a}$$

$$\alpha=-2\cos\frac{q}{2}\left(-2v^2q^2+3(1+\mathrm{i}\eta vq)\left(1+2\sin^2\frac{q}{2}\right)\right), \tag{34b}$$

$$\beta=3(1+\mathrm{i}\eta vq)^2\left(1+3\sin^2\frac{q}{2}\right)-4(1+\mathrm{i}\eta vq)v^2q^2\left(1+\sin^2\frac{q}{2}\right)+v^4q^4. \tag{34c}$$

Similarly, the even part of the determinant in the numerator becomes

$$\frac{F(\xi)}{1+\mathrm{i}\eta vq}, \tag{35}$$

with

$$F(\xi)=3\left[\left(\xi-(1+\mathrm{i}\eta vq)\cos\frac{q}{2}\right)^2+2(1+\mathrm{i}\eta vq)\sin^2\frac{q}{2}\left(1+\cos\frac{q}{2}\right)\right.$$
$$\left.\times(1+\mathrm{i}\eta vq-\xi)\right]-v^2q^2\left[(1+\mathrm{i}\eta vq)\left(1+\cos\frac{q}{2}\right)-\xi\cos\frac{q}{2}+1+\mathrm{i}\eta vq\right]. \tag{36}$$

We also write here the odd part of this determinant for future reference,

$$G(w)=\mathrm{i}\left(\frac{1}{w}-w\right)\sin\frac{q}{2}\left[v^2q^2-3(1+\mathrm{i}\eta vq)\sin^2\frac{q}{2}\right]. \tag{37}$$

Inserting Eqs. (33) and (35) into Eq. (32), we can see that Eq. (26) becomes

$$Q^{\mathrm{F}}(q)=\frac{N(q)}{2\pi\mathrm{i}(1+\mathrm{i}\eta vq)}\oint_{w=1}\frac{\mathrm{d}w}{w}\frac{F(\xi)}{3\xi^2+\alpha\xi+\beta} \tag{38}$$

with the integration around the unit circle taken in the counter-clockwise direction. The integrand in Eq. (33) has three poles inside the unit circle; i.e., $w=0$ and one w for each of the two roots of the quadratic in Eq. (33),

$$\xi_{1,2} = C \pm \sqrt{C^2 - D} \tag{39}$$

with

$$C = \cos\frac{q}{2}\left[-\frac{2}{3}v^2q^2 + (1+\mathrm{i}\eta vq)\left(1+2\sin^2\frac{q}{2}\right)\right], \tag{40a}$$

$$D = (1+\mathrm{i}\eta vq)^2\left(1+3\sin^2\frac{q}{2}\right) - \frac{4}{3}(1+\mathrm{i}\eta vq)v^2q^2\left(1+\sin^2\frac{q}{2}\right) + \frac{1}{3}v^4q^4. \tag{40b}$$

Then calculating the residues at these poles we get

$$Q^{\mathrm{F}}(q) = \frac{N(q)}{1+\mathrm{i}\eta vq}(1-S) \tag{41}$$

where

$$S(q) = \frac{F(\xi_1)\sqrt{\xi_2^2-(1+\mathrm{i}\eta vq)^2} - F(\xi_2)\sqrt{\xi_1^2-(1+\mathrm{i}\eta vq)^2}}{3(\xi_1-\xi_2)\sqrt{\xi_1^2-(1+\mathrm{i}\eta vq)^2}\sqrt{\xi_2^2-(1+\mathrm{i}\eta vq)^2}}. \tag{42}$$

Note that we are supposed to take those branches of the square roots in Eq. (42) that ensure that

$$|w_{1,2}| < 1 \tag{43}$$

with $w_{1,2}$ defined by

$$w_{1,2} = \frac{\xi_{1,2} - \sqrt{\xi_{1,2}^2-(1+\mathrm{i}\eta vq)^2}}{(1+\mathrm{i}\eta vq)}. \tag{44}$$

If we now substitute $N(q)$ from Eq. (41) into Eq. (18), we get

$$Q^+ + SQ^- + \frac{\eta v}{1+\mathrm{i}\eta vq}(1-S)Q(0) = \frac{(1-S)P_0^-}{1+\mathrm{i}\eta vq}. \tag{45}$$

We have now to choose P_0, our external forcing. In taking the width to infinity, in essence we are solving for the "inner" solution in the sense of boundary-layer theory; i.e., only on the scale of the lattice spacing. The external forcing in the finite width problem only acts on the large scale, and does not vary on the lattice scale. Thus, P_0 must have support only at $q=0$. Following Slepyan, then, we choose P_0 such that

$$\frac{1-S}{S^+(1+\mathrm{i}\eta vq)}P_0^- = 2\pi B\delta(q) = B\left(\frac{1}{\mathrm{i}q+0^+} + \frac{1}{-\mathrm{i}q+0^+}\right), \tag{46}$$

where B is a constant. This then gives us the two separate equations

$$Q^+ = -\frac{\eta vQ(0)}{1+\mathrm{i}\eta vq}\left(1-\frac{S^+}{S^+|_{q=\mathrm{i}/\eta v}}\right) + \frac{BS^+}{-\mathrm{i}q+0^+}, \tag{47a}$$

$$Q^- = -\frac{\eta v Q(0)}{1+\mathrm{i}\eta v q}\left(\frac{1}{S^- S^+|_{q=\mathrm{i}/\eta v}} - 1\right) + \frac{B}{(\mathrm{i}q+0^+)S^-}. \tag{47b}$$

As shown in Eqs. (86) and (88), we can solve for $Q(0)$ from either Eq. (47a) or (47b) by multiplying the first by $-\mathrm{i}q \to +\infty$ or the second by $\mathrm{i}q \to +\infty$. This yields

$$Q(0) = BS^+|_{q=\mathrm{i}/\eta v}. \tag{48}$$

Substituting this back into Eqs. (47), we find

$$Q^+ = \frac{BS^+}{(-\mathrm{i}q+0^+)(1+\mathrm{i}\eta v q)} - \frac{\eta v B}{1+\mathrm{i}\eta v q} S^+|_{q=\mathrm{i}/\eta v}, \tag{49a}$$

$$Q^- = \frac{B}{(-\mathrm{i}q+0^+)(1+\mathrm{i}\eta v q)S^-} + \frac{\eta v B}{1+\mathrm{i}\eta v q} S^+|_{q=\mathrm{i}/\eta v} S^-. \tag{49b}$$

These equations directly determine the displacements given the strength of the external driving, B. To get a physical handle on the meaning of this constant, we note that Eqs. (47) can be directly solved for the leading behavior of $Q^\pm$ as q goes to 0, using the fact that, in this limit,

$$S^\pm \sim \kappa^{\pm 1}\sqrt{A(q \pm \mathrm{i}0^+)}, \tag{50}$$

where

$$A = \frac{1}{\sqrt{2}v^2}\left(\frac{\sqrt{\frac{3}{8}-v^2}}{2} - \frac{(-\frac{3}{4}+v^2)^2}{\sqrt{3}\sqrt{\frac{9}{8}-v^2}}\right) \tag{51}$$

and κ is a constant, reflecting the arbitrariness in how we perform the decomposition of S. This expression for A contains the transverse speed $c_\mathrm{t} = \sqrt{3/8}$ and longitudinal speed $c_\mathrm{l} = \sqrt{9/8}$. As we shall see, the zero of A gives the limiting speed of crack propagation, $c_\mathrm{R} = (3-\sqrt{3})/2 = 0.563$, which is as expected equal to the Raleigh wave speed. Using Eq. (50), the limit of the Q's is seen to be

$$Q^+ \sim \kappa\sqrt{A}\frac{\mathrm{i}^{1/2}B}{(\mathrm{i}q+0^+)^{1/2}}, \tag{52a}$$

$$Q^- \sim \frac{\kappa}{\sqrt{A}}\frac{\mathrm{i}^{1/2}B}{(\mathrm{i}q+0^+)^{3/2}}. \tag{52b}$$

This is just the expected (Fourier transform of the) the singular solution of continuum elasticity as one approaches the crack tip. Thus, as in all boundary-layer problems, the large-distance limit of the "inner" solution matches on to the short-distance limit of the "outer" solution, confirming the argument for the choice of F_0 above. We need to relate the strength of the short-distance singularity of the continuum solution to the driving displacement Δ. This can be done directly by solving the continuum elastic equations. It is easier, however, to follow Slepyan and derive this relation by

energy considerations. One can calculate (Slepyan, 1981) the flux of energy into the boundary-layer, or "process" zone, obtaining

$$T = \frac{\mathrm{i}\kappa^2 B^2}{2} v. \tag{53}$$

Now consider the flux of energy T_0 being used to break bonds, which is simply related to $V(0)$:

$$T_0 = \frac{(BS^+|_{q=\mathrm{i}/\eta v})^2}{2} v. \tag{54}$$

Then, using the fact that the Griffith's displacement, Δ_{G}, is determined by the condition that at this value the energy flux is just exactly that needed to break the bonds and that the energy flux is proportional to the square of the externally applied driving displacement Δ, we have

$$\frac{\Delta}{\Delta_{\mathrm{G}}} = \sqrt{\frac{T}{T_0}} = \frac{\mathrm{i}^{1/2}\kappa}{S^+|_{q=\mathrm{i}/\eta v}}. \tag{55}$$

Notice that the factor of κ guarantees that the result is invariant with respect to how the decomposition of S is performed.

4. Numerical calculation of steady-state solutions

In this section we derive an integral form for the basic result, Eq. (55). We then present a numerical procedure for finding the displacement–velocity curve. The basic notion is to utilize Eq. (91) from the appendix to find S^+. It is more convenient for the numerical work to isolate explicitly the singularity at $q = 0$, defining $K(q)$ by

$$K(q) \equiv \frac{S^2(q)(q^2 + \phi^2)}{A^2(q + \mathrm{i}0^+)(q - \mathrm{i}0^+)\phi^2}. \tag{56}$$

where ϕ is an arbitrary positive constant. Because of the factor A^2q^2 in the denominator, $K(0) = 1$; the factor $(q^2 + \phi^2)/\phi^2$ does not alter the desired asymptotic behavior at infinity: $K \to const$ as $q \to \infty$. Applying Eq. (91), we get for $Im\, q > 0$:

$$S^+ = \exp\frac{1}{4\pi\mathrm{i}} \int_{-\infty}^{\infty} \mathrm{d}\gamma \, \frac{\ln S^2(\gamma)}{\gamma - q} = \left(A\phi \, \frac{q + \mathrm{i}0^+}{q + \mathrm{i}\phi}\right)^{1/2} (K^+)^{1/2}; \tag{57}$$

and for $Im\, q < 0$:

$$\frac{1}{S^-} = \exp\frac{1}{4\pi\mathrm{i}} \int_{-\infty}^{\infty} \mathrm{d}\gamma \, \frac{\ln S^2(\gamma)}{\gamma - q} = \left(\frac{1}{A\phi} \, \frac{q - \mathrm{i}\phi}{q - \mathrm{i}0^+}\right)^{1/2} (K^-)^{-1/2}, \tag{58}$$

with

$$(K^{\pm})^{\pm 1/2} = \exp\frac{1}{4\pi \mathrm{i}} \int_{-\infty}^{\infty} \mathrm{d}\gamma \, \frac{\ln K(\gamma)}{\gamma - q}, \tag{59}$$

where the upper sign is for $Im\, q > 0$ and the lower sign for $Im\, q < 0$.

As $K(0) = 1$, there is no pole in the integral in Eq. (59) at $\gamma = 0$ when $q = 0$. This means that $K^{+}(0) = (K^{-}(0))^{-1}$ and the asymptotic expressions for $S^{\pm}$ are

$$S^{+}|_{q\to 0} = \sqrt{\frac{AK^{+}(0)}{\mathrm{i}}(q + \mathrm{i}0^{+})^{1/2}}; \quad S^{-}|_{q\to 0} = \sqrt{\frac{\mathrm{i}A}{K^{+}(0)}(q - \mathrm{i}0^{+})^{1/2}}. \tag{60}$$

Comparing this to Eq. (50), we have

$$\kappa = \sqrt{-\mathrm{i}K^{+}(0)}, \tag{61}$$

so that Eq. (55) translates to

$$\frac{\Delta}{\Delta_{\mathrm{G}}} = \sqrt{\frac{1 + \phi\eta v}{A\phi} \frac{K^{+}(0)}{K^{+}(\mathrm{i}/\eta v)}}. \tag{62}$$

Explicitly writing out the integrals, we get

$$\frac{\Delta}{\Delta_{\mathrm{G}}} = \sqrt{\frac{1 + \phi\eta v}{A\phi}} \exp\frac{1}{4\pi \mathrm{i}} \int_{-\infty}^{\infty} \mathrm{d}\gamma \frac{\ln K(\gamma)}{\gamma(1 + \mathrm{i}\eta v\gamma)}. \tag{63}$$

The extra degree of convergence of the integrand at infinity is very desirable, as it helps control the fact that $\ln K(\xi)$ is a rapidly oscillating function. Also, the fact that the answer must be independent of ϕ provides a check on the numerical routines. A change of variables $\gamma \to -\gamma$ allows the integral to be rewritten so that

$$\frac{\Delta}{\Delta_{\mathrm{G}}} = \sqrt{\frac{1 + \phi\eta v}{A\phi}} \exp\frac{1}{4\pi} \int_{0}^{\infty} \mathrm{d}\gamma \, Im \, \frac{\ln K(\gamma)}{\gamma(1 + \mathrm{i}\eta v\gamma)}. \tag{64}$$

This form makes clear that as A approaches 0, Δ diverges, confirming our above remark about the Rayleigh wave speed being the limiting velocity.

To actually compute this integral, we divided the region of integration into two parts, from 0 to 1 and from 1 to $+\infty$. The second integral was further transformed so as to have in the numerator the factor $\ln A^2\phi^2 K(\xi)$, which goes to zero at infinity; the subtracted integral with the numerator $\ln 1/(A\phi)^2$ was performed analytically. After all these manipulations, the integrals were successfully computed by standard mathematical library subroutines.

The results of these calculations are presented in Figs. 2 and 3. These findings are quite similar to the analogous mode III results (Kessler, 2000). Later, we will show that the upper limiting value of $\Delta/\Delta_{\mathrm{G}}$ for an arrested (i.e., lattice-trapped (Thomson, 1986)) crack is around 1.94. As was the case for mode III, the $\Delta - v$ curves in Figs. 2, 3 approach this value as v goes to 0 at any value of the damping η. Slepyan's original calculations, done for the dissipationless limit $\eta = 0$, show the same asymptotic value.

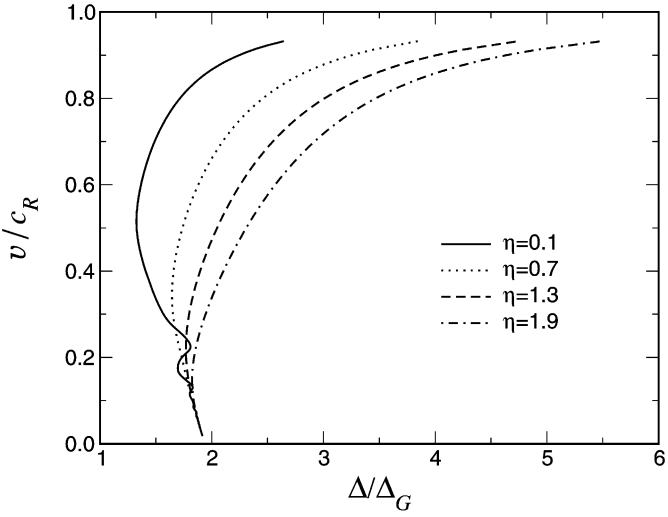

Fig. 2. Dependence of crack speed v on the dimensionless driving Δ/Δ_G, for varying dissipation: $\eta = 0.1, 0.7, 1.3, 1.9$.

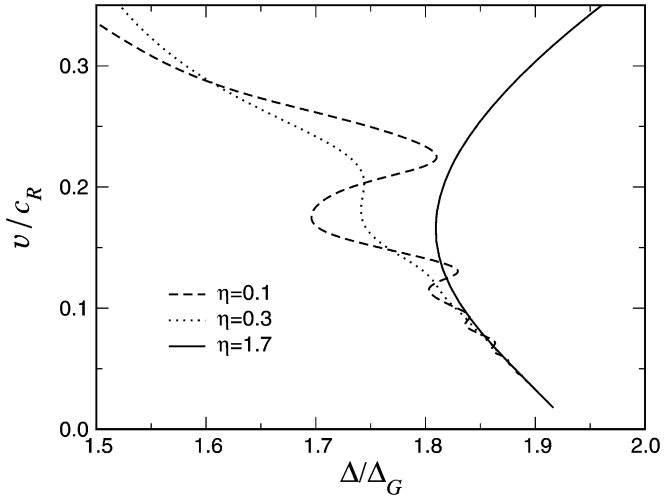

Fig. 3. Change in behavior in the velocity–driving curve as η is made small. Note the rapid oscillations at smaller speeds.

5. Consistency of the steady-state solution

As mentioned in the Introduction, cracks are seen to become unstable above a critical velocity. In the framework of the model being considered here, one might assume that this velocity is associated with the solution as found by the Wiener–Hopf method

becoming inconsistent (Marder and Liu, 1993). As we shall see, there are two kinds of inconsistencies. The first sets in for small v, for small enough η. Here the vertical bond between $y=0$ and 1 first achieves critical extension prematurely, at some positive τ, contradicting the assumption that the bond breaks at $\tau=0$. In the second kind of inconsistency, a bond off the crack path achieves critical extension. If the model is defined so that only the vertical bonds between $y=0$ and 1 are breakable, then this does not present a problem. If on the other hand, all the springs are chosen to be identical, so that the horizontal springs and other vertical springs also break at the same critical extension as the vertical ones, then the solution is indeed inconsistent at this point. This is what occurs at large enough velocity, for all η.

To proceed, we must calculate the bond lengths, transforming back our Fourier space solutions so as to obtain the physical displacements. Let us start with bonds along the crack path, where the elongation is straightforwardly determined by transforming $Q^{\mathrm{F}}(q)$ back to physical space. From Eqs. (47) and (48), we easily obtain for $Q^{\pm}$:

$$Q^{+}=\frac{Q(0)}{(-\mathrm{i}q+0^{+})(1+\mathrm{i}\eta vq)}\frac{S^{+}}{S^{+}|_{q=\mathrm{i}/\eta v}}-\frac{\eta vQ(0)}{1+\mathrm{i}\eta vq}, \tag{65a}$$

$$Q^{-}=\frac{Q(0)}{(\mathrm{i}q+0^{+})(1+\mathrm{i}\eta vq)}\frac{1}{S^{-}S^{+}|_{q=\mathrm{i}/\eta v}}+\frac{\eta vQ(0)}{1+\mathrm{i}\eta vq}. \tag{65b}$$

and for $Q(\tau)$:

$$Q(\tau>0)=Q(0)\int_{-\infty}^{\infty}\frac{\mathrm{d}q}{2\pi}\frac{\sqrt{A\phi}\mathrm{e}^{-\mathrm{i}q\tau}}{\sqrt{(\mathrm{i}q-0^{+})(\mathrm{i}q-\phi)}(1+\mathrm{i}\eta vq)}\frac{(K^{+})^{1/2}}{S^{+}|_{q=\mathrm{i}/\eta v}}, \tag{66a}$$

$$\begin{aligned}Q(\tau<0)=&\,Q(0)\mathrm{e}^{\tau/\eta v}\\&+Q(0)\int_{-\infty}^{\infty}\frac{\mathrm{d}q}{2\pi}\frac{\mathrm{e}^{-\mathrm{i}q\tau}}{\sqrt{A\phi}(\mathrm{i}q+0^{+})(1+\mathrm{i}\eta vq)}\left(\frac{\mathrm{i}q+\phi}{\mathrm{i}q+0^{+}}\right)\frac{(K^{-})^{-1/2}}{S^{+}|_{q=\mathrm{i}/\eta v}}.\end{aligned} \tag{66b}$$

Clearly, these integrals must be performed numerically. To proceed, we transform the pieces containing the factors $K^{\pm}$ by dividing both the numerator and denominator by $(K^{+}(0))^{1/2}$. In the denominator, we get $\Delta/\Delta_{\mathrm{G}}$; we have already discussed how this can be computed. We now have integrands containing factors of the form

$$\frac{(K^{+}(q))^{\pm1/2}}{(K^{+}(0))^{1/2}}=\exp\frac{1}{4\pi\mathrm{i}}\int_{-\infty}^{\infty}\mathrm{d}\xi\,\frac{q\ln K(\xi)}{\xi(\xi-q)}. \tag{67}$$

The $\pm$ on the right-hand side refers to the sign of the imaginary part of q. As we will see later on, we need to calculate this function only for positive q. Then, the integral in the exponent can be written as

$$\frac{1}{2\pi\mathrm{i}}\int_{0}^{\infty}\mathrm{d}\xi\frac{Re\ln K(q\xi)}{\xi^{2}-(1\pm\mathrm{i}0^{+})^{2}}+\frac{1}{2\pi}\int_{0}^{\infty}\mathrm{d}\xi\frac{Im\ln K(q\xi)}{\xi(\xi^{2}-(1\pm\mathrm{i}0^{+})^{2})}. \tag{68}$$

We break up the region of integrations into three parts, $(0,1/2),(1/2,3/2)$ and $(3/2,+\infty)$. In the first interval, we numerically calculate the integral directly as

written. For the third interval, we proceed as discussed in the last section for a similar semi-infinite integral; this leaves us with having to integrate numerically a function that behaves as $1/\xi^4$ near infinity. Finally, for the integral near 1 we add an integral with $K(q\xi)$ replaced by $K(q)$; this added integral is done analytically and the resultant subtracted integral with the integrand now containing $\ln K(q\xi)/K(q)$ is done numerically.

Applying the described procedure, we can evaluate the functions $(K^{\pm}(q))^{\pm 1/2}/(K^{+}(0))^{1/2}$ for any real positive q. We must now perform the final integration over the variable q. First, we note that the requirement of having a real displacement necessitates $V^{\pm}(-q) = V^{\pm}(q)^*$. This allows us to change the region of integration to $(0, +\infty)$ in Eq. (66a); we will return shortly to Eq. (66b). The trickiest part of this calculation concerns the behavior near $q = 0$. For V^{+}, there is a $1/q^{1/2}$ behavior. Here the leading order term can be integrated analytically over the interval $(0, 1)$ and then the overall function with this term subtracted can be used for a numerical integration. This works in a straightforward manner.

We need to be more careful with the integral in Eq. (66b) because here the integrand behaves near zero as $1/q^{3/2}$. To proceed, we first divide the interval of integration into three parts; $(-\infty, -1)$, $(-1, 1)$, and $(1, +\infty)$. The integrals over $(-\infty, -1)$ and $(1, +\infty)$ can again be combined to yield an integral of twice the real part of the integrand over the latter range. For the range spanning zero, we first subtract from the integrand the leading term $A^{-1/2}(\mathrm{i}q + 0^{+})^{-3/2}/S^{+}|_{q=\mathrm{i}/\eta v}$. After this subtraction, the integrand becomes of order $1/q^{1/2}$. Now, the one-sided integral converges, and thus we can again transform the range to $(0, 1)$. This subtracted integral is evaluated numerically from a very small value of q (typically $q = 10^{-3}$) to 1. In the remaining part of the range, i.e., from 0 to 10^{-3}, we evaluate the integral analytically after approximating it by its leading small q behavior, $\alpha/q^{1/2}$; the value of the constant α is determined by fitting the behavior of the function near the point 10^{-3}. Finally we need to perform analytically the integral of the subtracted piece $A^{-1/2}(\mathrm{i}q + 0^{+})^{-3/2}/S^{+}|_{q=\mathrm{i}/\eta v}$. To accomplish this, we deform the contour of integration from $(-1, 1)$ on the real axis to the curve from -1 to 1 going over the lower half of the unit circle. Note that the branch-cut for this function must be taken as before over the negative real axis; this choice guarantees the fact that $f(-q) = f^*(q)$. Note that once all our transformations are complete, we only need values for the integrand for positive (real) values of q; this was used earlier in the technique for calculating $K^{\pm}$. A good check of this complex numerical technique of computing the Fourier transformation is applying it to the Fourier transform $Q^{+}(q)$ for $\tau < 0$ and $Q^{-}(q)$ for $\tau > 0$, as in these cases the result must be equal to zero.

This calculation gives us the elongation of the vertical bonds crossing the crack surface. The results are shown in Fig. 4. A careful examination shows that as the velocity is decreased the function becomes more oscillatory. This is similar to what is known to occur for mode III (Marder and Gross, 1995; Kessler, 2000). For small enough velocity, the magnitude of the oscillations is sufficiently great that the bond extension exceeds the critical extension (taken here to be 1) at positive τ, i.e., *before* the time it was assumed to crack. This inconsistency at low v and small η was already noted by Marder and Gross (1995). As η increases, the oscillations are increasingly

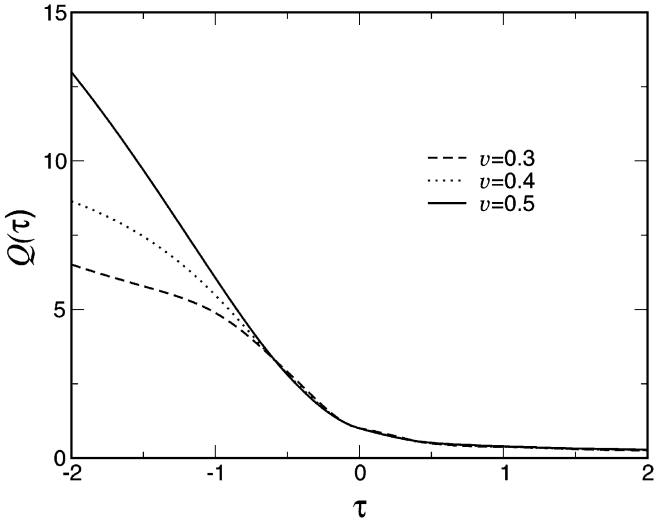

Fig. 4. Elongation of bonds on the crack surface, $Q(\tau)$ for $\eta = 0.5$. Results are shown for three velocities, $v = 0.3, 0.4, 0.5$.

damped, so that for sufficiently large η, of order 1, the oscillations are completely overdamped and the inconsistency disappears.

At large velocities, bonds off the crack line can exceed critical extension. We begin with the horizontal bond elongations above the crack line (e.g., the bond labeled "c" in Fig. 1) or equivalently, below, which requires us to calculate a different component of the displacement (than the one which goes into Q). In detail, we have

$$Q_{\mathrm{h}}(q) \equiv Q_1^{\mathrm{F}}(q, n=0) = \frac{\sqrt{3}}{4\pi} \int_{-2\pi/\sqrt{3}}^{2\pi/\sqrt{3}} \mathrm{d}s (\mathrm{e}^{-\mathrm{i}\vec{r}\cdot\hat{d}_1} - 1) \vec{u}^{\,\mathrm{FF}} \cdot \hat{d}_1$$
$$= (\mathrm{e}^{-\mathrm{i}q} - 1) \frac{\sqrt{3}}{4\pi} \int_{-2\pi/\sqrt{3}}^{2\pi/\sqrt{3}} \mathrm{d}s \, \frac{\det \boldsymbol{M}_1}{\det \boldsymbol{M}}, \tag{69}$$

where these matrices were defined in the last section.

We now proceed as before to change variables to w and rewrite this expression in terms of the auxiliary variable ξ defined in Eq. (34a).

$$\det M_1 = -\frac{N(q)H(\xi)}{1 + \mathrm{i}\eta v q} + \text{term odd in } s, \tag{70}$$

where

$$H(\xi) = \frac{3}{2}(1 - \mathrm{e}^{\mathrm{i}q/2})(1 + \mathrm{i}\eta v q + \xi) \left(1 + \mathrm{i}\eta v q - \xi \cos\frac{q}{2} - \frac{v^2 q^2}{3}\right)$$
$$- \frac{3\mathrm{i}}{2} \sin\frac{q}{2} (1 + \mathrm{e}^{\mathrm{i}q/2})(\xi^2 - (1 + \mathrm{i}\eta v q)^2). \tag{71}$$

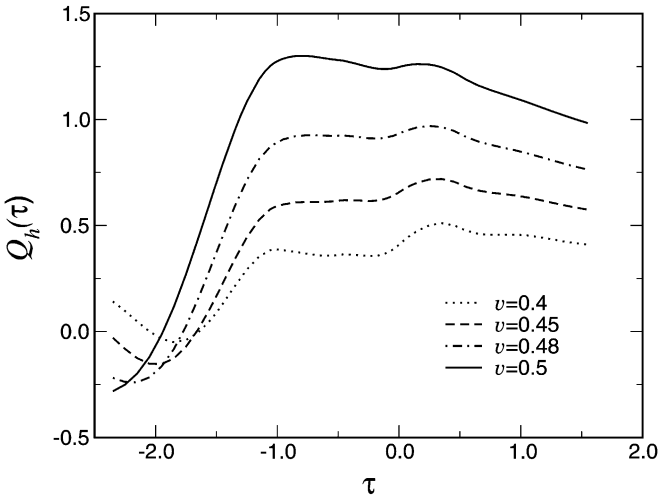

Fig. 5. Elongation of the horizontal bonds, $Q_{\rm h}(\tau)$, for $\eta = 0.1$; results are shown for four velocities, $v = 0.4, 0.45, 0.48, 0.5$. The instability sets in whenever $Q_{\rm h}$ exceeds unity.

As before, the integrand in Eq. (69) has three poles. Dropping the irrelevant odd term and performing the integral leads to the expression

$$Q_{\rm h}(q) = \frac{N(q)}{1 + {\rm i}\eta v q}(1 - {\rm e}^{-{\rm i}q})\psi_{\rm h}(q) \tag{72}$$

with

$$\psi_{\rm h}(q) = \frac{1 - {\rm e}^{{\rm i}q/2}}{2} - \frac{H(\xi_1)\sqrt{\xi_2^2 - (1 + {\rm i}\eta v q)^2} - H(\xi_2)\sqrt{\xi_1^2 - (1 + {\rm i}\eta v q)^2}}{3(\xi_1 - \xi_2)\sqrt{\xi_1^2 - (1 + {\rm i}\eta v q)^2}\sqrt{\xi_2^2 - (1 + {\rm i}\eta v q)^2}}. \tag{73}$$

Branches of the square root satisfy the same conditions (43), (44), as earlier. The function $N(q)$ can be found from Eq. (41)

$$N(q) = \frac{(1 + {\rm i}\eta v q)Q^{\rm F}(q)}{1 - S}. \tag{74}$$

Our final answer is

$$Q_{\rm h}(q) = \frac{Q(0)}{S^+|_{q={\rm i}/\eta v}S^-}\frac{(1 - {\rm e}^{-{\rm i}q})\psi_{\rm h}(q)}{({\rm i}q + 0^+)(1 + {\rm i}\eta v q)}. \tag{75}$$

For q close to 0, the function $(1-{\rm e}^{-{\rm i}q})\psi_{\rm h}(q)$ behaves as q, giving a divergence $1/q^{1/2}$ for $Q_{\rm h}(q)$. This is similar to the divergence in $Q^+(q)$. Thus, the numerical calculation of $Q_{\rm h}(\tau)$ is similar to the calculation of $Q(\tau)$ for $\tau > 0$. Fig. 5 displays $Q_{\rm h}(\tau)$ for several values of η and v. Generally speaking, the function $Q_{\rm h}(\tau)$ has maxima in two different places, one somewhere in the vicinity of -1 and a second for $\tau > 0$.

We also need to find the bond elongation between the layers with $n = 1$ and 2 and between the layers with $n = -1$ and 0. Due to symmetry (31) it is sufficient to consider only $Q_2^{\rm F}\ (q, n = \pm 1)$, which we will denote as $Q_{\pm}(q)$. The bond labeled "a" in Fig. 1 corresponds to Q_-. We can derive for it an expression similar to that in Eq. (38) with

the major difference being that in this case the odd parts of the explicit determinant in Eq. (32) do not cancel out because of the additional factor $w^{\pm 1}$:

$$Q_{\pm}(q) = \frac{N(q)}{2\pi \mathrm{i}} \oint_{w=1} \frac{\mathrm{d}w}{w} w^{\pm 1} \frac{F(\xi)/(1+\mathrm{i}\eta v q) + G(w)}{3\xi^2 + \alpha\xi + \beta}$$

$$= \frac{N(q)}{2\pi \mathrm{i}} \oint_{w=1} \mathrm{d}w \frac{F(\xi)/(1+\mathrm{i}\eta v q) \pm G(w)}{3\xi^2 + \alpha\xi + \beta}. \tag{76}$$

To derive the second equality, we used a change of variables $w \to 1/w$, along with the symmetries of F and G. Again the integration in Eq. (76) is in the counter-clockwise direction. In this case, the integrand in the second form of the integral has just two poles inside the unit sphere, at $w_{1,2}$. After the by now familiar tedious calculations, we find

$$Q_{\pm}(q) = \frac{N(q)}{1+\mathrm{i}\eta v q} \psi_{\pm}(q), \tag{77}$$

where

$$\psi_{\pm}(q) = -\frac{F(\xi_1) w_1}{3(\xi_1 - \xi_2)\sqrt{\xi_1^2 - (1+\mathrm{i}\eta v q)^2}} + \frac{F(\xi_2) w_2}{3(\xi_1 - \xi_2)\sqrt{\xi_2^2 - (1+\mathrm{i}\eta v q)^2}}$$

$$\pm \frac{g(q)(w_1 - w_2)}{3(\xi_1 - \xi_2)} \tag{78}$$

with

$$g(q) = -2\mathrm{i} \sin\frac{q}{2}\left[v^2 q^2 - 3(1+\mathrm{i}\eta v q)\sin^2\frac{q}{2}\right] \tag{79}$$

and $N(q)$ is again given by Eq. (74). Finally we obtain

$$Q_{\pm}(q) = \frac{Q(0)}{S^+|_{q=\mathrm{i}/\eta v} S^-} \frac{\psi_{\pm}(q)}{(\mathrm{i}q + 0^+)(1+\mathrm{i}\eta v q)}. \tag{80}$$

Just as was the case for $Q_{\mathrm{h}}(q)$ and $Q^+(q)$, $Q_{\pm}(q)$ behaves as $1/q^{1/2}$ near 0. Thus numerical calculations can be performed just as in the previous cases. Fig. 6 shows several curves $Q_{\pm}(\tau)$ for differing parameters.

Given the elongations of these "vulnerable" bonds, we can investigate the critical speed at which one of these bonds should be broken. Fig. 7 shows the results of our calculations of this critical speed. In Fig. 8 we plot τ_{cr} at which these bonds break; this allows us to identify the spatial and time coordinates of breaking and enable us to make contact with our finite lattice calculations later. We found that the maximum value of $Q_-(\tau)$ always reaches 1 before $Q_+(\tau)$ and that this is the most dangerous bond for small dissipation. This curve turns around at an η of around 1.2, so that $Q_-(\tau)$ is always subcritical for larger η. This is a result of the fact that the maximum value of $Q_-(\tau)$ is, surprisingly enough, not monotonic with velocity, but reaches a maximum and then decreases with increasing velocity. The maximum extension of this type of bond occurs, for large velocity, at some distance from the

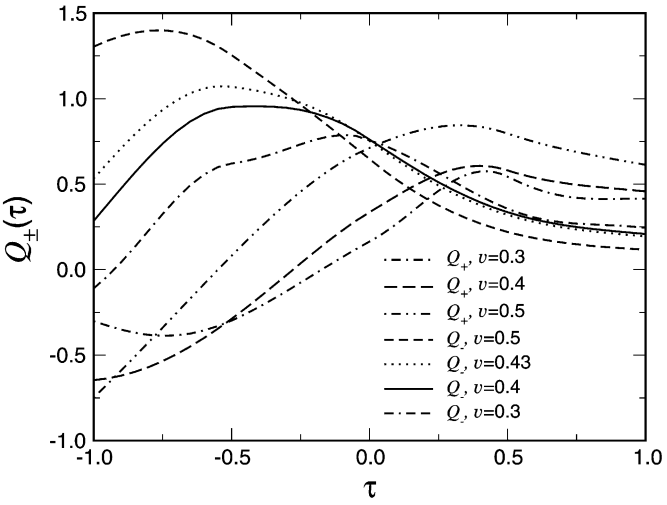

Fig. 6. Elongation of bonds on the layer above and below the crack layer, $Q_{\pm}(\tau)$ for $\eta = 0.1$. Again, instability corresponds to elongation $Q > 1$.

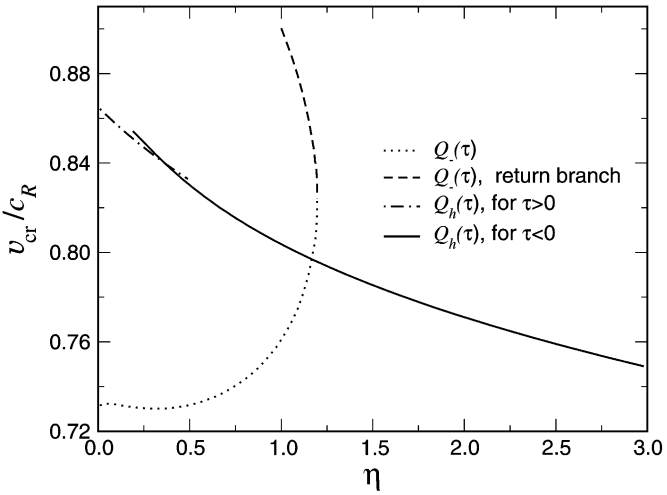

Fig. 7. Critical speed v_{cr} for instability onset for various bonds; horizontal, and above and below the crack surface.

crack surface. For small η, where the maximum $Q_-(\tau)$ does exceed critical extension, the decrease of the maximum Q_- with v restabilizes the bond beyond some velocity. The dominant threshold for η above about 1.1, then, comes from the horizontal bond breaking. Note that as η increases, the critical velocity decreases. Also, for small η, a

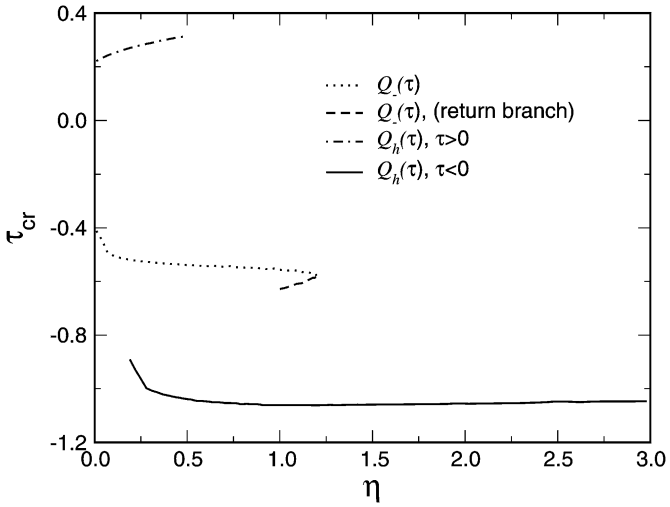

Fig. 8. Time of bond breaking at the critical speed.

crossover occurs as the relative importance of the two different maxima in the horizontal bond elongation reverse; this region is anyway irrelevant as the next-layer vertical bond breaks at a lower velocity. Whenever the horizontal bond dominates, the maximum at $\tau \cong -1$ is the governing one. As we see from Fig. 8, even for large η this critical τ stays near -1, what means that the horizontal bond always breaks near, and slightly behind, the tip of the crack.

Many of these features appear to be special to the Mode I problem, with no analog in Mode III calculations. At least for the Mode III square lattice case, horizontal bond breaking always dominates (Pechenik, 2000) and furthermore the maximum bond extension off the crack surface is a strictly increasing function of the velocity. This points to the possibility that the dynamics of Mode I may be much richer than the Mode III dynamics.

6. Finite lattice model

For our Mode III calculations, it proved interesting to compare the exact results derived for an infinite lattice with the numerical determination of crack propagation properties in lattices of small transverse size (Kessler and Levine, 1998; Kessler, 2000). We now discuss similar calculations for our Mode I model. In addition to providing details regarding the size needed to attain answers relevant to the macroscopic limit (a question of direct relevance for direct molecular dynamics simulations (Abraham et al., 1994; Gumbsch et al., 1997; Holland and Marder, 1997, 1998; Omeltchenko et al., 1997; Zhou et al., 1997), for example), finite lattice results can be used as a rough

check on some of the predictions obtained above. Given the complexity of the analysis, having such a check is quite useful.

6.1. Arrested crack

Let us start with trying to find arrested cracks, expected to exist in some range of the driving Δ around the Griffith's displacement. This involves looking for a solution of Eq. (1) with $\vec{u}(x, y)$ independent of time and with the forces on the right-hand side arising solely from the broken bonds. If we have a system with a finite number of rows, the natural boundary condition requires that the top and bottom rows have fixed vertical displacements of Δ and $-\Delta$, respectively. Since the entire system is linear, we can choose to use $\Delta = 1$ and rescale the breaking criterion accordingly.

Since we are a numerical calculation, we must introduce artificial boundaries in the direction along the crack, $\hat{x}$. We do this by cutting off the range of points whose coordinates are variables and outside of this range impose fixed asymptotic displacements. On the cracked side, these are just $\vec{u} = \pm\,\Delta\hat{y}$ for positive and negative y. On the uncracked side, the asymptotic displacement corresponds to constant strain. At each of the sites that has a variable displacement, we impose the two components of the (vectorial) equation of motion. We also impose the equations of motion at the boundaries of the system. This gives us more equations than we have variables. The coupling of sites which contain variable displacements with the ones with fixed displacements gives rise to inhomogeneous terms. Combining these observations, we can write our system in the schematic form $Mu - b = 0$, with a non-square matrix M. The field u is then determined by the requirement that the error be minimal. In this manner, the small errors introduced at the boundary by having to have a fixed box size are prevented from causing any large errors (via modes which grow exponentially away from the edges) in the bulk of the lattice.

The solution of this linear system determines the elongation of all bonds. In Fig. 9 we show a typical lattice given by this solution. In fact we need to know the elongation of just two bonds right at the tip of the crack; the one which in the case of the moving crack would break next (Q_n) and the other which would have been the last one broken (Q_l). Now, recall that we have scaled our displacement to equal unity and the only remaining displacement scale is the elongation at which the springs break, which we can call ε. The solution we have found is consistent as long as ε is between the lower limit set by the Q_n and the upper limit set by Q_l. Since $\Delta_\mathrm{G} = \varepsilon\sqrt{(2N+1)/3}$, where $2N$ is the number of rows in the y-direction (excluding the boundary rows whose displacement is constrained), we directly obtain the upper and lower limits of the arrested crack band:

$$\frac{1}{Q_\mathrm{l}\sqrt{\frac{1}{3}(2N+1)}} \leqslant \frac{\Delta}{\Delta_\mathrm{G}} \leqslant \frac{1}{Q_\mathrm{n}\sqrt{\frac{1}{3}(2N+1)}}. \tag{81}$$

The results for these thresholds as a function of lattice size are shown in Figs. 10 and 11. In the limit of an infinite lattice, the lower limiting value $\Delta_-/\Delta_\mathrm{G}$ approaches 0.515, while the upper limiting value $\Delta_+/\Delta_\mathrm{G}$ approaches 1.94.

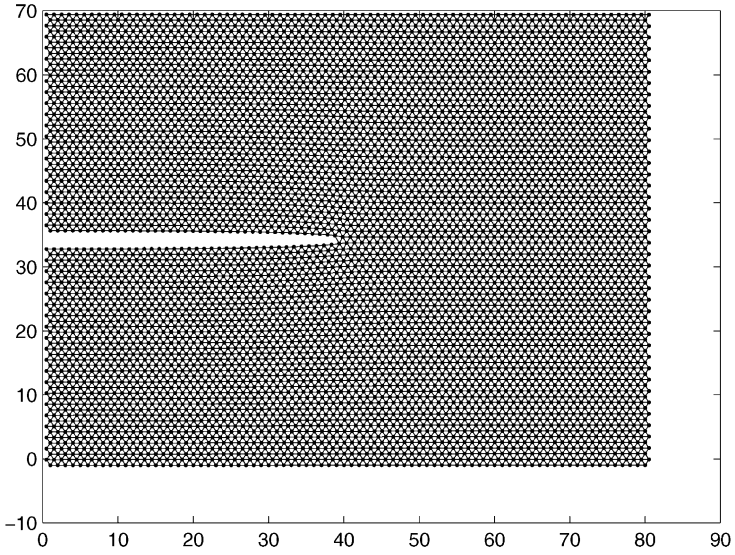

Fig. 9. Solution for an arrested crack in a finite width lattice model.

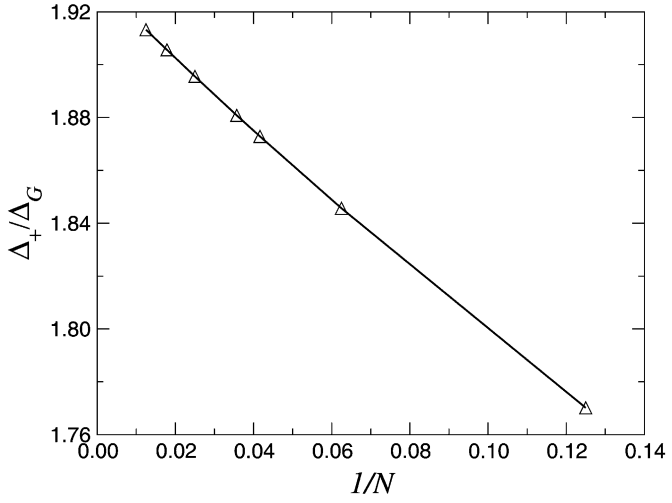

Fig. 10. Upper limiting Δ for a Mode I arrested crack in a triangular lattice, as a function of lattice width.

6.2. Stable moving cracks

We now turn to the moving crack problem. Again, we need to solve Eq. (1) with the forces on the right-hand side due to the broken bonds. Now, the displacement field $\vec{u}(x, y, t)$ is of course time dependent. Therefore, we need to introduce a time-step Δt

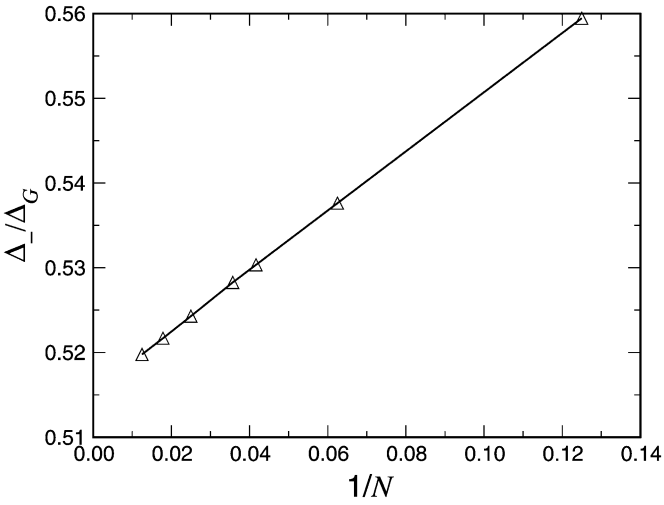

Fig. 11. Lower limiting Δ for a Mode I arrested crack in a triangular lattice, as a function of lattice width.

so as to define the time-points at which we will obtain a numerical solution. Given some specific speed v of the crack, we choose to divide half of the time interval that it takes for the crack to propagate one lattice spacing, $1/(2v)$, into n equal time intervals; thus $\Delta t = 1/(2vn)$. Now we can discretize our system, obtaining equations at times $t = 0,\ \Delta t, \ldots, (n-1)\Delta t$. We use a symmetric discretization of first and second derivatives $(\vec{u}(t+\Delta t) - \vec{u}(t-\Delta t))/(2\Delta t)$ and $(\vec{u}(t+\Delta t) - 2\vec{u}(t) + \vec{u}(t-\Delta t))/(\Delta t)^2$, respectively. These equations depend on displacements $\vec{u}$ outside of this time interval, because of the temporal derivatives. These can be found via use of the assumed symmetries of the moving crack; in fact, it is easy to see that we thereby trade in displacements outside of the modeled interval with displacements inside this interval albeit at a different spatial location. The boundaries are treated the same way as described for the arrested crack; the displacements outside some range are replaced by asymptotic values for all of the time-points in our interval. Including the equations at these boundary points again gives us a system in which the number of equations exceeds the number of variables and again a least squared error algorithm is used to find the required solution.

We used these finite lattice calculations to provide an independent check on our analytic infinite lattice results. We were specifically interested in checking the critical speed estimates. The difficulty is that convergence in the parameter $1/N$ is fairly slow and using large lattices is rather time-consuming and memory-demanding. In practice, we limited our calculations to N's ranging from 6 to 24. It turns out that for small dissipation where it is the next-row vertical bond vulnerability which determines the critical velocity, we can do a credible job of verifying that the infinite lattice results are consistent with the finite lattice ones. For example, in Fig. 12, we show the critical speed as a function of lattice size for several different values of η. These numbers, if extrapolated to infinite N are clearly consistent with the results given earlier in Fig. 7,

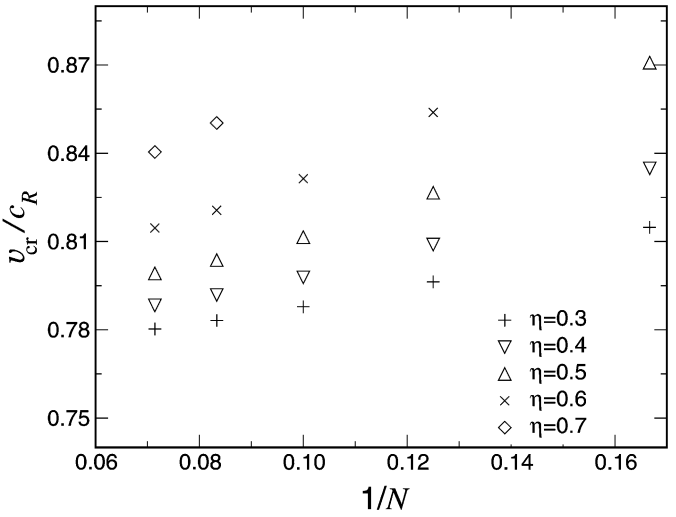

Fig. 12. Critical speed due to the vertical bond breaking on the layer next to the crack; data are presented as a function of lattice width parameter N.

especially considering that having a finite time-step introduces a small numerical error on its own. We can also check the critical time τ at which the bond breaking occurs. From Fig. 8, we see that in the infinite lattice the break occurs for $\tau \sim -0.5$. For the finite lattice with $n = 5$, this means that the bond "a" highlighted in Fig. 1 should go above breaking threshold at the first time-point of the modeled interval. This is exactly what occurs.

A different strategy is necessary for studying the onset of horizontal bond breaking. This is due to the fact that quite large N's are required in to order for the results to quantitatively approach the infinite N limit. As a result, the picture of which bonds are critical changes dramatically between finite N and the infinite N limit. In Fig. 13, we present the "phase diagram" for critical bonds for $N = 38$, plotted together with the infinite N result, and in Fig. 14, we compare the $N = 38$ results to those for $N = 26$. Since the steady-state code is difficult to run at these large values of N, the data in these two plots were obtained from time-dependent simulations, with only the central vertical bonds allowed to break. After running to times of $t = 100$ to eliminate transients, the extensions of the dangerous bonds were checked to see if they exceeded criticality. Note that, in contradistinction to the "phase diagram" plotted in Fig. 7, we now plot Δ/Δ_G on the vertical axis, since this is the input control parameter for the simulations. We see that qualitative behavior of the "Q_-" bonds is similar to the infinite-N result, with these bonds being below critical extension for both large η and large Δ/Δ_G. The horizontal bonds also behave qualitatively like their infinite-N counterparts, but the quantitative agreement, is as we noted above, significantly worse. In fact, for large η, the most dangerous bond is in fact of "Q_+" type. However, the threshold at which the "Q_+" type bond becomes dominant is pushed to larger η as the system size is increased, presumably going to infinity with N. Also, there is a small region of η

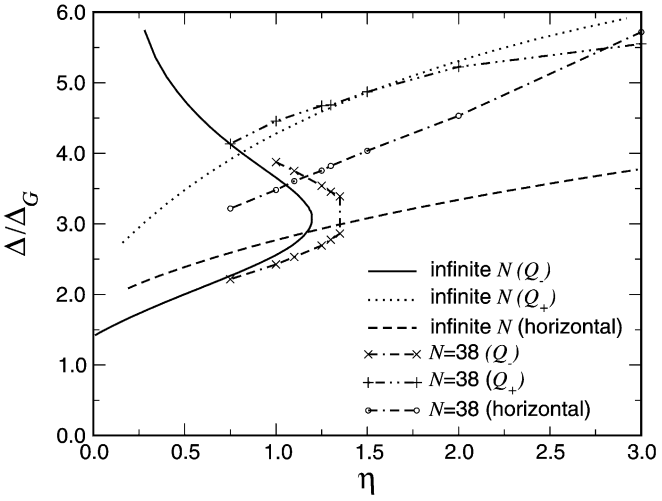

Fig. 13. Comparison of the driving thresholds for critical bond extension for $N = \infty$ and 38.

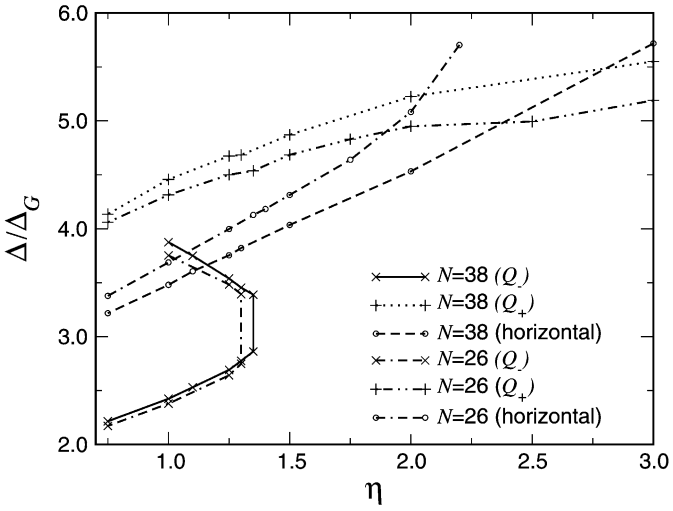

Fig. 14. Comparison of the driving thresholds for critical bond extension for $N = 38$ and 26.

around 1.1 where the inconsistency is re-entrant, so that for intermediate values of Δ, no bonds of the crack surface are critical. Thus, to see dynamics qualitatively representative of the macroscopic system requires very large system sizes at moderate to large η. Presumably, this is connected to the process zone increasing in size with η. This leads to the conclusion that in molecular dynamics simulations, the width of the material taken should be very large to accurately study the micro-branching instability.

7. Discussion

In this work, we have discussed steady-state mode I crack propagation in a viscoelastic lattice model. Our primary method of analysis utilizes the Wiener–Hopf technique to write down closed form expressions for both the v–Δ curves (for various values of the dissipation η) and for the bond elongation field. The latter enables us to obtain the limit of consistency for the solution past which some bonds that are not along the crack path have elongations greater than the assumed breaking criterion. These results are new, and correspond to non-trivial extensions of the v–Δ curve in the dissipationless limit by Kulamekhtova et al. (1984) in the infinite width case and by Marder and Gross (1995) for small lattices.

The most interesting results, in our opinion, concern the dependence of the critical velocity (where the aforementioned inconsistency sets in) on the amount of dissipation. For small dissipation, this threshold is relatively insensitive to η, as already suggested in direct numerical simulations (Pla et al., 1998). This threshold, occurring at roughly 0.73 of the Rayleigh speed is in some ways reminiscent of the Yoffe (1951) branching criterion which suggests that straight crack propagation will become unstable once the largest stress direction shifts away from being straight ahead. It is unfortunately hard to be more precise regarding this correspondence since the crack dynamics in our model is fundamentally tied to the lattice scale, not the macroscopic scale—in fact, the latter is completely invisible in the Slepyan approach aside from providing a driving force in the form of a stress intensity factor.

At larger η, the instability picture changes. Now, it is a horizontal bond breaking which signals the onset of more complex crack dynamics. Also, the threshold goes down with increasing dissipation. This appears to be a new instability, as it is strongly dissipation dependent and is not associated with crack branching.

Much of the recent theoretical work on Mode I cracks has been motivated by experiments which show clearly that instabilities limit the range of steady-state crack propagation. These instabilities introduce more complex spatio-temporal dynamics to the fracture process, causing additional dissipation and leaving behind a roughened crack surface. It has been tempting to associate these results with the onset of inconsistencies in lattice models, although the details of this correspondence remain uncertain. First, most of the experimental work has been carried out in amorphous materials, for which the idea of an ordered lattice model is somewhat suspect. These experiments seem to show a typical frequency for micro-branching which is not connected in any obvious way to dynamics at a lattice scale. The instabilities seen experimentally typically occur at smaller speeds than the ones seen in lattice systems with small dissipation and indeed at smaller speeds than one sees in fracture experiments carried out on single crystal materials (Cramer et al., 1999; Field, 1971; Hauch et al., 1999). There is however, recent evidence that single crystal experiments exhibit three-dimensional effects that clearly cannot be captured in any 2d model (Cramer et al., 2000).

Notwithstanding all these issues, we remain optimistic that the study of this class of models will lead to insight into dynamic fracture. There are several intriguing possibilities that need to be investigated in the future. First, we have shown that for mode I cracks, increasing the dissipation (in the form of a Kelvin viscosity) eventually

results in a decrease of the instability threshold. If our model is really applied at the atomic scale, it is hard to see why there should be a large linear dissipation; on the other hand, it is well known that lattice models miss an essential non-linear dissipation mechanism, namely the creation of dislocations that remain pinned to the crack. Would inclusion of these effects also lower the threshold? Of course, dislocations come with their own complex dynamics and one would need to understand much better than we do at present as to how these dynamics interact with the crack tip.

On the other hand, applying the model on a large scale (possibly for a disordered system) would naturally require a large dissipation and recent numerical simulations indicate that proper inclusion of the thermal fluctuations might also push the model into better agreement with experiment (Pla et al., 1998; Sander and Ghasias, 1999). Finally, the exact nature of the state which occurs past the instability onset has not been addressed in our work to date, and in fact cannot be addressed by the elegant but ultimately limiting analytic methods utilized for the steady-state problem. Instead, we plan to study a generalized force law in which the sharp breaking criterion is replaced by an analytic non-linear force versus displacement (Kessler and Levine, 1999). In this formulation, the inconsistency found here becomes a linear instability of the steady-state crack (Kessler and Levine, 2001) and one can use some of the methods developed in the field of nonequilibrium pattern formation to unravel the dynamics past onset. These studies, together with additional experimental data regarding the differences between brittle fracture in crystalline versus non-crystalline materials, will hopefully lead to a better understanding of dynamic fracture.

Acknowledgements

D.A.K. acknowledges the support of the Israel Science Foundation. The work of H.L. and L.P. is supported in part by the NSF, grant no. DMR94-15460. D.A.K. and L.P. thank Prof. A. Chorin and the Lawrence Berkeley National Laboratory for their hospitality during the initial phase of this work.

Appendix A. conventions and notations

We discuss here some of our conventions and notations regarding Fourier transformations. We use Fourier transformation in the form

$$u^{\mathrm{F}}(q) = \int_{-\infty}^{\infty} \mathrm{d}\tau\, u(\tau) \mathrm{e}^{\mathrm{i}q\tau},$$

$$u(\tau) = \frac{1}{2\pi} \int_{-\infty}^{\infty} \mathrm{d}q\, u^{\mathrm{F}}(q) \mathrm{e}^{-\mathrm{i}q\tau}. \tag{82}$$

We also define u^+ and u^- as

$$u^+(q) = \int_0^\infty \mathrm{d}\tau\, u(\tau)\mathrm{e}^{\mathrm{i}q\tau}, \tag{83a}$$

$$u^-(q) = \int_{-\infty}^0 \mathrm{d}\tau\, u(\tau)\mathrm{e}^{\mathrm{i}q\tau}. \tag{83b}$$

This gives

$$u(\tau)\theta(\tau) = \frac{1}{2\pi}\int_{-\infty}^\infty \mathrm{d}q\, u^+(q)\mathrm{e}^{-\mathrm{i}q\tau}.., \tag{84a}$$

$$u(\tau)\theta(-\tau) = \frac{1}{2\pi}\int_{-\infty}^\infty \mathrm{d}q\, u^-(q)\mathrm{e}^{-\mathrm{i}q\tau}, \tag{84b}$$

which means that u^+ has poles only in the lower half plane and u^- only in the upper half plane.

Now let us define $p = -\mathrm{i}q$. Then,

$$\int_0^\infty \mathrm{d}\tau\, u(\tau)\mathrm{e}^{\mathrm{i}q\,\tau} \overset{p\to+\infty}{\sim} u(0)\int_0^\infty \mathrm{d}\tau\, \mathrm{e}^{-p\tau} = \frac{u(0)}{p}. \tag{85}$$

Thus

$$\lim_{-\mathrm{i}q\to+\infty} -\mathrm{i}qu^+ = u(0). \tag{86}$$

Similarly we can get for $p = \mathrm{i}q$

$$\int_{-\infty}^0 \mathrm{d}\tau\, u(\tau)\mathrm{e}^{\mathrm{i}q\tau} \overset{p\to+\infty}{\sim} u(0)\int_{-\infty}^0 \mathrm{d}\tau\, \mathrm{e}^{p\tau} = \frac{u(0)}{p}, \tag{87}$$

giving

$$\lim_{\mathrm{i}q\to+\infty} \mathrm{i}qu^- = u(0). \tag{88}$$

The Fourier transform of $\theta(-\tau)\mathrm{d}/\mathrm{d}\tau\, u(\tau)$ is given by

$$\int_{-\infty}^0 \mathrm{d}\tau\, \frac{\mathrm{d}u(\tau)}{\mathrm{d}\tau}\mathrm{e}^{\mathrm{i}q\tau} = u(0) - \mathrm{i}qu^-. \tag{89}$$

Finally, we consider separating an arbitrary function $S(q)$ into the product of two pieces S^+ and S^- with poles and zeroes in the lower and upper half planes, respectively. This can be done using the identity

$$\begin{aligned}\frac{1}{2\pi\mathrm{i}}\int_{-\infty}^\infty \mathrm{d}\xi\, \frac{\ln S(\xi)}{\xi - q} &= \frac{1}{2\pi\mathrm{i}}\int_{-\infty}^\infty \mathrm{d}\xi \left(\frac{\ln S^+(\xi)}{\xi - q} + \frac{\ln S^-(\xi)}{\xi - q}\right) \\ &= \begin{cases} \textit{for } \mathrm{Im}\, q > 0, & \ln S^+(q) \\ \textit{for } \mathrm{Im}\, q < 0, & \ln S^-(q). \end{cases}\end{aligned} \tag{90}$$

References

Abraham, F.F., Brodbeck, D., Rafey, R.A., Rudge, W.E., 1994. Instability dynamics of fracture—a computer-simulation investigation. Phys. Rev. Lett. 73 (2), 272–275.

Barenblatt, G.I., 1959. The formation of equilibrium cracks during brittle fracture: general ideas and hypothesis, axially symmetric cracks. Appl. Math. Mech. 23, 622–636.

Cramer, T., Wanner, A., Gumbsch, P., 1999. Dynamic fracture of glass and single crystalline Silicon. Z. Metallkd 90, 675–686.

Cramer, T., Wanner, A., Gumbsch, P., 2000. Energy dissipation and path instabilities in dynamic fracture of Silicon single crystals. Phys. Rev. Lett. 85 (4), 788–791.

Field, J.E., 1971. Brittle fracture: its study and application. Contemp. Phys. 12, 1–13.

Fineberg, J., Gross, S.P., Marder, M., Swinney, H.L., 1991. Instability in dynamic fracture. Phys. Rev. Lett. 67 (4), 457–460.

Fineberg, J., Gross, S.P., Marder, M., Swinney, H.L., 1992. Instability in the propagation of fast cracks. Phys. Rev. B 45 (10), 5146–5154.

Fineberg, J., Marder, M., 1999. Instability in dynamic fracture. Phys. Rep. 313 (1–2), 1–108.

Gumbsch, P., Zhou, S.J., Holian, B.L., 1997. Molecular dynamics investigation of dynamic crack stability. Phys. Rev. B 55 (6), 3445–3455.

Hauch, J.A., Holland, D., Marder, M.P., Swinney, H.L., 1999. Dynamic fracture in single crystal Silicon. Phys. Rev. Lett. 82 (19), 3823–3826.

Holland, D., Marder, M., 1997. Ideal brittle fracture of silicon studied with molecular dynamics. Phys. Rev. Lett. 80 (4), 746–749.

Holland, D., Marder, M., 1998. Erratum: ideal brittle fracture of silicon studied with molecular dynamics. Phys. Rev. Lett. 81 (18), 4029.

Kessler, D.A., 2000. Steady-state cracks in viscoelastic lattice models II. Phys. Rev. E 61 (3), 2348–2360.

Kessler, D.A., Levine, H., 1998. Steady-state cracks in viscoelastic lattice models. Phys. Rev. E 59 (5), 5154–5164.

Kessler, D.A., Levine, H., 1999. Arrested cracks in nonlinear lattice models of brittle fracture. Phys. Rev. E 60 (6), 7569–7571.

Kessler, D.A., Levine, H., 2001. Nonlinear lattice models of viscoelastic mode-III fracture. Phys. Rev. E 63 (1) No. 016118/1–9.

Kulamekhtova, Sh.A., Saraikin, V.A., Slepyan, L.I., 1984. Plane problem of a crack in a lattice. Izv. AN SSSR. Mekh. Tverd. Tela 19 (3) 112–118 [Mech. Solids 19 (3), 102–108].

Langer, J.S., 1992. Models of crack propagation. Phys. Rev. E 46 (6), 3123–3131.

Langer, J.S., Lobkovsky, A.E., 1998. Critical examination of cohesive-zone models in the theory of dynamic fracture. JPSP 46 (9), 1521–1556.

Marder, M., Gross, S.P., 1995. Origin of crack tip instabilities. J. Mech. Phys. Solids 43 (1), 1–48.

Marder, M., Liu, X., 1993. Instability in lattice fracture. Phys. Rev. Lett. 71 (15), 2417–2420.

Omeltchenko, A., Yu, J., Kalia, R.K., Vashishta, P., 1997. Crack front propagation and fracture in a graphite sheet: a molecular-dynamics study on parallel computers. Phys. Rev. Lett. 78 (11), 2148–2151.

Pechenik, L., 2000. Pattern formation and nonlinear dynamics in nonequilibrium physical systems. Ph.D. Thesis, UCSD, 2000.

Pla, O., Guinea, F., Louis, E., Ghasias, S.V., Sander, L.M., 1998. Viscous effects in brittle fracture. Phys. Rev. B 57 (22), R13,981–R13,984.

Sander, L.M., Ghasias, S.V., 1999. Thermal noise and the branching threshold in brittle fracture. Phys. Rev. Lett. 83 (10), 1994–1997.

Sharon, E., Gross, S.P., Fineberg, J., 1995. Local crack branching as a mechanism for instability in dynamic fracture. Phys. Rev. Lett. 74 (25), 5096–5099.

Sharon, E., Gross, S.P., Fineberg, J., 1996. Energy dissipation in dynamic fracture. Phys. Rev. Lett. 76 (12), 2117–2120.

Slepyan, L.I., 1981. Dynamics of a crack in a lattice. Dokl. Akad. Nauk SSSR 258 (1–3) 561–564 [Sov. Phys.-Dokl. 26 (5), 538–540].

Slepyan, L.I., 1982. The relation between the solutions of mixed dynamical problems for a continuous elastic medium and a lattice. Dokl. Akad. Nauk SSSR 266 (1–3), 581–584 [Sov. Phys.-Dokl. 27 (9), 771–772].

Slepyan, L.I., Ayzenburg–Stepanenko, M.V., Dempsey, J.P., 1999. Mech. Time-Dependent Mater. 3, 159–203.

Thomson, R., 1986. The physics of fracture. Solid State Phys. 39, 1–29.

Yoffe, E.H., 1951. The moving griffith crack. Philos. Mag. 42 (7), 739–750.

Zhou, S.J., Beazley, D.M., Lomdahl, P.S., Holian, B.L., 1997. Large-scale molecular dynamics simulations of three-dimensional ductile failure. Phys. Rev. Lett. 78 (3), 479–482.